Computers in Biology and Medicine 108 (2019) 200–212

Contents lists available at ScienceDirect

Computers in Biology and Medicine

journal homepage: www.elsevier.com/locate/compbiomed

Multiscale modeling of the cardiovascular system for infants, children, and adolescents: Age-related alterations in cardiovascular parameters and hemodynamics

Xiancheng Zhang[a,b], Hideaki Haneishi[b], Hao Liu[a,c,*]

[a] Graduate School of Engineering, Chiba University, Inage, Chiba, Japan
[b] Center for Frontier Medical Engineering, Chiba University, Inage, Chiba, Japan
[c] Shanghai Jiao Tong University and Chiba University International Cooperative Research Center (SJTU-CU ICRC), Minhang District, Shanghai, China

ARTICLE INFO

Keywords:
Multiscale cardiovascular model
Age-related cardiovascular parameters and hemodynamics
Allometric scaling law
Global sensitivity analysis

ABSTRACT

While zero- and one-dimensional multiscale modeling of the adult cardiovascular system (CVS) has been recognized as a useful tool in cardiovascular research and clinical applications, there are still not any generic cardiovascular models for a broad range of age groups. To study age-related alterations in cardiovascular parameters and hemodynamics, we here presented a versatile multiscale cardiovascular model considering the cardiovascular growth and development during aging. An adult cardiovascular model was first established by utilizing population-averaged physiological data. We then introduced an allometric scaling law-based approach to estimate age-related cardiovascular parameters for infants, children, and adolescents, by using the newly defined scaling exponents for different types of cardiovascular parameters. The model was validated to be capable of predicting the age-related alterations in hemodynamics through a comprehensive comparison with available *in vivo* measurements. Moreover, a variance-based global sensitivity analysis was performed for all cardiovascular parameters under normal and abnormal conditions to identify which are the most important model inputs in affecting model outputs. Our results indicate that the present generic cardiovascular model provides a robust and useful tool for evaluating normal cardiovascular functions over a broad age range for biomedical engineering applications.

1. Introduction

The 0-1D multiscale cardiovascular model has been a promising tool for the simulation-based predictive medicine to aid clinicians in unveiling the association between complex pathophysiologic mechanisms of cardiovascular diseases and hemodynamics [1–5], because of its versatility and robustness in the global hemodynamic analysis and pulse wave analysis, as well as in providing physiologically adequate boundary conditions for the 3D image-based hemodynamic simulation. However, previously developed cardiovascular models are primarily about the adult cardiovascular system (CVS); a cardiovascular model applicable for predicting hemodynamics over a broad age range is still lacking, and thus limiting their applicability on computer-aided hemodynamic predictions.

Clinical observations report that over 50% of the patients with cardiac surgeries are within 0–19 years old [6], for instance, the staged Fontan operation is usually accomplished at 0.2–5 years old [7]. Moreover, the youngest children usually show a highest post-operative mortality, such as the 6-months mortality after cardiac surgery is nearly 10% [6]. Therefore, developing a multiscale cardiovascular model applicable to a broad age range, in particular involving infants and children, would be of great physiological and clinical significance.

Obviously, the increasing body size with aging inevitably results in significant changes in cardiovascular parameters, which are characterized by the increase in the vessel size (diameter and length), vessel stiffness (pulse wave velocity), heart size (mass and volume), total vascular compliance, and total blood volume, while it causes a decrease in the cardiac systolic performance, heart rate, and total vascular resistance [8–17]. On the other hand, the age-related alterations in cardiovascular parameters cause significant changes in hemodynamics. The biggest challenge in developing a multiscale cardiovascular model adaptive to a broad age range arises from the lack of sufficient physiological data for defining cardiovascular model parameters. It is very challenging or even infeasible to collect data of the cardiovascular

* Corresponding author. Graduate School of Engineering, Chiba University, 1-33, Yayoi-cho, Inage-ku, Chiba, Japan.
E-mail address: hliu@faculty.chiba-u.jp (H. Liu).

https://doi.org/10.1016/j.compbiomed.2019.03.021
Received 15 January 2019; Received in revised form 24 February 2019; Accepted 21 March 2019

Nomenclature

0-1D	Zero- and one-dimensional
3D	Three dimensional
CVS	Cardiovascular system
ASL	Allometric scaling law
SA	Sensitivity analysis
UQ	Uncertainty quantification
S_m	Main sensitivity index
LHS	Latin Hypercube Sampling
C	Vascular compliance ($ml{\cdot}mmHg^{-1}$)
R	Vascular resistance ($mmHg{\cdot}s{\cdot}ml^{-1}$)
V	Blood volume (ml)
Z	Characteristic impendence ($mmHg{\cdot}s{\cdot}ml^{-1}$)
q	Blood flow rate ($ml{\cdot}s^{-1}$)
$\bar{q}$	Cycle-averaged flow rate ($ml{\cdot}s^{-1}$)
p	Blood pressure (mmHg)
P_0	Reference pressure (mmHg)
A_0	Vascular cross-sectional area at P_0 (cm^2)
D_0	Vascular diameter at P_0 (cm)
Len	Vessel length (cm)
c_0 (PWV)	Pulse wave velocity ($m{\cdot}s^{-1}$)
ρ	Blood density ($kg{\cdot}m^{-3}$)
E	Elastance ($mmHg{\cdot}ml^{-1}$)
E_a	Active elastance amplitude ($mmHg{\cdot}ml^{-1}$)
E_p	Passive elastance baseline ($mmHg{\cdot}ml^{-1}$)
V_0	Unstressed volume (ml)
V_{ini}	Initial volume (ml)
V_{pe}	Pericardial volume (ml)
V_{pc0}	Pericardial volume offset (ml)
ϕ_{pc}	Pericardial volume constant (ml)
S	Viscoelasticity ($mmHg{\cdot}s{\cdot}ml^{-1}$)
ϕ_S	Viscoelasticity constant ($s{\cdot}ml^{-1}$)
D_{cv}	Diameter of the cardiac valve (cm)
l_{cv}	Length of the cardiac valve (cm)
$A_{eff,max}$	Maximum effective cross-sectional area at valve is fully open (cm^2)
$A_{eff,min}$	Minimum effective cross-sectional area at valve is fully closed (cm^2)
K_{vo}	Valve opening rate coefficients ($mmHg^{-1}{\cdot}s^{-1}$)
K_{vc}	Valve closing rate coefficients ($mmHg^{-1}{\cdot}s^{-1}$)
L	Inertance ($mmHg{\cdot}s^2{\cdot}ml^{-1}$)
B	Bernoulli's resistance ($mmHg{\cdot}s^2{\cdot}ml^{-2}$)
p_{pc}	Pericardial pressure (mmHg)
p_{it}	Intrathoracic pressure (mmHg)
X	Cardiovascular parameter
W	Body weight (kg)
α	Normalization constant
β	Scaling exponent
TAPSE	Tricuspid annular plane systolic excursion
SV	Stroke volume (ml)
CO	Cardiac output ($L{\cdot}min^{-1}$)
MAP	Mean systemic artery pressure (mmHg)
HR	Heart rate (min^{-1})
mP	Mean blood pressure (mmHg)
mP_{as}	Mean ascending aortic pressure (mmHg)
mP_{ivc}	Mean inferior vena caval pressure (mmHg)
mP_{mpua}	Mean main pulmonary artery pressure (mmHg)
mP_{rpua}	mean right pulmonary artery pressure (mmHg)
t_{vcp}	Duration of ventricular contraction (s)
t_{ar}	Timing of atrial relaxation (s)
AscAo	Ascending Aorta
AoArc I	Aortic Arch I
BCA	Brachiocephalic Artery
AoArc II	Aortic Arch II
LCA	Left Carotid Artery
LSA	Left Subclavian Artery
DTA	Descending Thoracic Aorta
IVC	Inferior Vena Cava
SVC	Superior Vena Cava
MPA	Main Pulmonary Artery
LPA	Left Pulmonary Artery
RPA	Right Pulmonary Artery
LSPA	Left Superior Pulmonary Artery
LIPA	Left Inferior Pulmonary Artery
RSPA	Right Superior Pulmonary Artery
RIPA	Right Inferior Pulmonary Artery
LSPV	Left Superior Pulmonary Vein
LIPV	Left Inferior Pulmonary Vein
RSPV	Right Superior Pulmonary Vein
RIPV	Right Inferior Pulmonary Vein
TCPC	Total cavopulmonary connection
EC	Extracardiac conduit

Subscripts

i	Number of terminal artery
j	Number of terminal vein
ra	Right atrium
rv	Right ventricle
la	Left atrium
lv	Left ventricle
tv	Tricuspid valve
pv	Pulmonary valve
mv	Mitral valve
av	Aortic valve
sa	Systemic artery
sv	Systemic vein
svb	Systemic vascular bed
pua	Pulmonary artery
puv	Pulmonary vein
pvb	Pulmonary vascular bed
art	Artery
ven	Vein
T	Total
ivc	Inferior vena cava

parameters sufficiently through direct *in vivo* measurements because of the technical obstacles and even the ethical issue, e.g., the difficulties in measuring the end-systolic elastance of the right ventricle (E_{rv}) due to the complicated geometry [11].

Aiming at investigating the age-related alterations in both cardiovascular parameters and hemodynamics associated with human cardiovascular growth and development, the allometric scaling law (ASL) [18,19], whereby a biological (cardiovascular) variable is related to the mass of the organism by a power law, is herein applied to estimate the age-related cardiovascular parameters values for infants, children, and adolescents. We first established a closed-loop 0-1D multiscale cardiovascular model for the adult CVS by using the population-averaged data from published literature. We then applied ASL-based scaling approach to estimate age-related cardiovascular parameters for infants, children and adolescents through introducing newly defined scaling exponents for different kinds of cardiovascular parameters, the age-specific model was validated via comparison with experimental measurements of healthy subjects over an age range of 0–18 years old. Finally, to make our model more reliable for the simulation-based hemodynamic prediction, a variance-based global sensitivity analysis (SA) was performed

for all cardiovascular parameters under normal and abnormal conditions.

2. Methods

2.1. A closed-loop 0-1D multiscale model of the adult CVS

In the proposed adult cardiovascular model, 20 larger vessels including aortas, vena cava, pulmonary arteries and veins are represented by 1D models, and the remainder vessels are lumped into the 0D peripheral vascular beds, as illustrated in Fig. 1a. The geometrical and mechanical data of the 1D cardiovascular network are summarized in Table A.1 for a population-averaged adult model with the height, weight and age to be 175 cm, 75 kg, and 20–30 years, respectively. The 0D vascular bed (Fig. 1b) consists of 3 elements, involving an arterial compliance (C_{sa}), a vascular resistance (R_{svb}), and a venous compliance (C_{sv}). The terminal arteries and veins are connected to the vascular bed with characteristic independences (Z_{art} or Z_{ven}). If the total systemic arterial and venous compliances ($C_{T,sa}$ and $C_{T,sv}$), the total pulmonary arterial and venous compliances ($C_{T,pua}$ and $C_{T,puv}$), the total systemic vascular resistance ($R_{T,svb}$) and pulmonary vascular resistance ($R_{T,pvb}$) are known, the arterial and venous compliances, as well as the resistance associated with different vascular bed compartments can be determined. Take the systemic vascular bed as an example (Fig. 1b), the vascular resistance (R^i_{svb}), arterial compliance (C^i_{sa}), and venous compliance (C^j_{sv}) can be calculated as [20]:

$$R^i_{svb} = R_{T,svb}\frac{\bar{q}_T}{\bar{q}_i} - Z^i_{art} - Z^j_{ven}, \tag{1}$$

$$C^i_{sa} = \left(C_{T,sa} - \sum_{i=1}^{7}\frac{A^i_0 Len_i}{\rho(c^i_0)^2}\right)\frac{\bar{q}_i}{\bar{q}_T}\left(\frac{R^i_{svb} + Z^i_{art}}{R^i_{svb}}\right), \tag{2}$$

$$C^j_{sv} = \left(C_{T,sv} - \sum_{j=8}^{9}\frac{A^j_0 Len_j}{\rho(c^j_0)^2}\right)\frac{\bar{q}_j}{\bar{q}_T}, \tag{3}$$

where i and j denote the numbers of the terminal artery and terminal vein, ρ the blood density, A_0 the cross-sectional area of the 1D blood vessel, Len the length of the 1D blood vessel, c_0 the pulse wave velocity (PWV), $\bar{q}_i$ and $\bar{q}_j$ the cycle-averaged flow rates of the outlet of the terminal artery and the inlet of the terminal vein, $\bar{q}_T$ the cycle-averaged flow rates of the inlet of the ascending aorta, respectively. The characteristic impedance is defined with $Z = \rho c_0/A_0$ and the calculated parameters values for 0D peripheral vascular beds are given in Table A.2.

With respect to the heart modeling, we model each of the four cardiac chambers with a time-varying capacitor (i.e. the well-established time-varying elastance model) [1] with consideration of the direct pressure coupling between left and right ventricles through interventricular septum [21] to estimate their hemodynamic characteristics, i.e., the pressure-volume relationship. The viscoelasticity of the four cardiac walls is each modeled as a pressure-dependent resistor [22]. The four cardiac valves are each modeled as a resistor and inductor in series, to simulate the hemodynamic characteristics (pressure-flow relationships) across the valves [23]. The physiological data of the cardiac chambers and valves are summarized in Table A.3. Details associated with the governing equations and solution methods for 1D vascular flow, bifurcation, cardiac chambers and valves, and peripheral vascular beds [2,5,24] are documented in Supplemental file 1. The cardiovascular model was written in Fortran 90 language.

2.2. ASL-based parameter estimations for infants, children and adolescents

Generally, a cardiovascular parameter X may be represented with a power function of the body weight W [18]

$$X = \alpha W^{\beta}, \tag{4}$$

where α is a normalization constant and β denotes the scaling exponent. Accordingly, given the body weight, the age-related cardiovascular model parameters values for infants, children and adolescents can be reasonably estimated from the adult model parameters values [19], such as

$$X = X_{adult}\left(\frac{W}{W_{adult}}\right)^{\beta}. \tag{5}$$

We adjusted and redefined the scaling exponents (β) values of estimating different types of cardiovascular parameters under study, as shown in Table 1. Fig. 2 compared the estimated cardiovascular parameters values of using the defined β with *in vivo* measurements [8–13].

2.3. Methodology of the global SA

Here we employ the Monte Carlo-based approach for SA. For the sake of simplification in description of the methodology, we simply represent the developed cardiovascular model as a black-box function, such as

$$Y = f(X), \tag{6}$$

where $\boldsymbol{Y} = (y_1, y_2, \ldots, y_m)$ and $\boldsymbol{X} = (x_1, x_2, \ldots, x_k)$ represent the model outputs and inputs, respectively. The uncertainties of the model inputs are represented by assuming that they are normally distributed within the uncertain domain according to a probability density function $\rho(x_i)$. If the model inputs x_i ($i = 1, \ldots, k$) are independent, the joint probability density function can be represented by

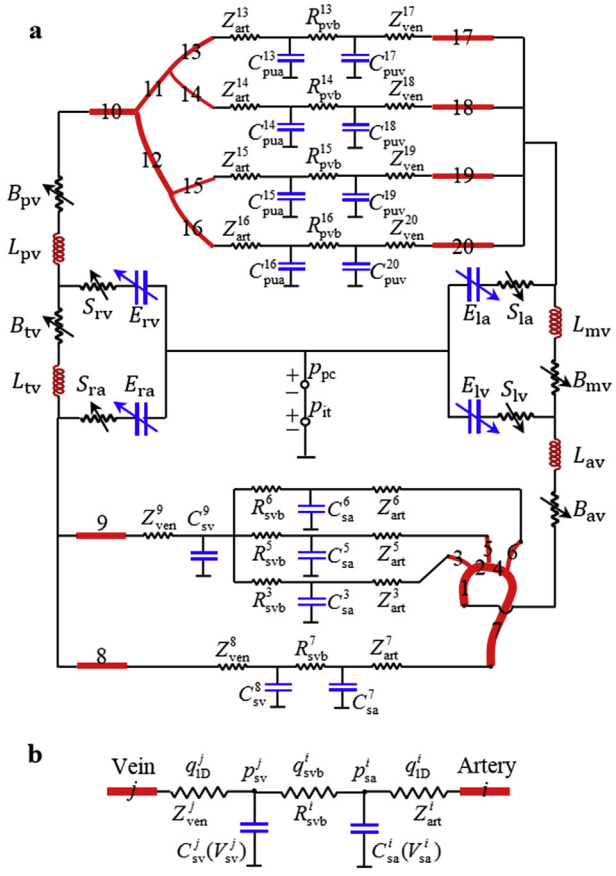

Fig. 1. Schematic representation of the computational model of the CVS. (a) The closed-loop 0-1D multiscale cardiovascular model. (b) A typical 0D vascular bed connected by a 1D terminal artery and a 1D terminal vein.

Table 1
A list of scaling exponents (β) associated with age-related cardiovascular parameters for infants, children, and adolescents.

Scaling exponent β	Cardiovascular parameter
For 1D cardiovascular network	
0.45	Vascular diameter (D_0) and length (Len)
Pulse wave velocity (c_0):	
0.2	Systemic arteries
0.065	Systemic veins
0.075	Pulmonary arteries
0.065	Pulmonary veins
0.1	Reference pressure (P_0)
For 0D cardiovascular model	
−0.475	Systemic vascular resistance ($R_{T,svb}$)
−0.7	Pulmonary vascular resistance ($R_{T,pvb}$)
1.0	Systemic arterial and venous compliances ($C_{T,sa}$ and $C_{T,sv}$)
	Pulmonary arterial and venous compliances ($C_{T,pua}$ and $C_{T,puv}$)
Cardiac elastance:	
−0.75	$E_{a,ra}$, $E_{p,ra}$
−0.5	$E_{a,la}$, $E_{p,la}$
−0.75	$E_{a,rv}$, $E_{p,rv}$
−0.5	$E_{a,lv}$, $E_{p,lv}$
0.45	Diameters and lengths of the four cardiac valves (D_{cv} and l_{cv})
−0.5	Valve opening and closing rate coefficients (K_{vo} and K_{vc})
−0.3	Heart rate
0.8	Blood volumes (V, V_{ini}, V_0, V_{pe}, V_{pc0}, ϕ_{pc})
1.0	Viscoelasticity (S)

$$\rho(x_1, x_2, \cdots, x_k) = \prod_{i=1}^{k} \rho(x_i), \tag{7}$$

and the expectation and variance of y are defined as

$$E(y) = \int_{\Omega_X} f(x_1, x_2, \cdots, x_k) \cdot \prod_{i=1}^{k} \rho(x_i) dx_i, \tag{8}$$

$$\mathrm{V}(y) = \int_{\Omega_X} f^2(x_1, x_2, \cdots, x_k) \cdot \prod_{i=1}^{k} \rho(x_i) dx_i - \mathrm{E}^2(y), \tag{9}$$

where Ω_X denotes the sample space of the model inputs. The values of model inputs and the corresponding uncertainties are listed in Supplemental file 2. We introduce the Latin Hypercube Sampling (LHS) technique to generate random samples for model inputs [25].

Following Saltelli's efficient procedure [26], the main sensitivity index (first order sensitivity index) is herein evaluated by

$$S_{m,i} = \frac{V[E(y|x_i)]}{V(y)}. \tag{10}$$

Evaluation of the term $S_{m,i}$ can be summarized as follows:

(1) Create two independent Latin Hypercube sample matrices $\boldsymbol{M}_1$ and $\boldsymbol{M}_2$ (each contains $n = 5000$ samples) for all of the model inputs

$$M_1 = \begin{bmatrix} x_1^{(1)} & x_2^{(1)} & \cdots & x_k^{(1)} \\ x_1^{(2)} & x_2^{(2)} & \cdots & x_k^{(2)} \\ \vdots & \vdots & \vdots & \vdots \\ x_1^{(n)} & x_2^{(n)} & \cdots & x_k^{(n)} \end{bmatrix}, \quad M_2 = \begin{bmatrix} x_1'^{(1)} & x_2'^{(1)} & \cdots & x_k'^{(1)} \\ x_1'^{(2)} & x_2'^{(2)} & \cdots & x_k'^{(2)} \\ \vdots & \vdots & \vdots & \vdots \\ x_1'^{(n)} & x_2'^{(n)} & \cdots & x_k'^{(n)} \end{bmatrix}; \tag{11}$$

(2) Create k sample matrices $\boldsymbol{N}_i$ ($i = 1, \ldots, k$) using $\boldsymbol{M}_1$ and $\boldsymbol{M}_2$. $\boldsymbol{N}_i$ can be generated by incorporating the i-th column of $\boldsymbol{M}_1$ into $\boldsymbol{M}_2$, such as

$$N_i = \begin{bmatrix} x_1'^{(1)} & x_2'^{(1)} & \cdots & x_i^{(1)} & \cdots & x_k'^{(1)} \\ x_1'^{(2)} & x_2'^{(2)} & \cdots & x_i^{(2)} & \cdots & x_k'^{(2)} \\ \vdots & \vdots & \vdots & \vdots & \vdots & \vdots \\ x_1'^{(n)} & x_2'^{(n)} & \cdots & x_i^{(n)} & \cdots & x_k'^{(n)} \end{bmatrix}; \tag{12}$$

(3) Run the cardiovascular code for each row of the generated $k+2$ sample matrices to get all of the model outputs;

(4) Evaluate main sensitivity indices $S_{m,i}$ for all model inputs with obtained model outputs in step (3), such as

$$S_{m,i} = \frac{U_i - E^2(y)}{V(y)}, \tag{13}$$

where

$$U_i = \frac{1}{n} \sum_{s=1}^{n} f(x_1^{(s)}, x_2^{(s)}, \cdots, x_k^{(s)}) \cdot f(x_1'^{(s)}, x_2'^{(s)}, \cdots, x_i^{(s)}, \cdots, x_k'^{(s)}), \tag{14}$$

$$E^2(y) = \frac{1}{n} \sum_{s=1}^{n} f(x_1^{(s)}, x_2^{(s)}, \cdots, x_k^{(s)}) \cdot f(x_1'^{(s)}, x_2'^{(s)}, \cdots, x_k'^{(s)}), \tag{15}$$

$$V(y) = \frac{1}{n} \sum_{s=1}^{n} f^2(x_1^{(s)}, x_2^{(s)}, \cdots, x_k^{(s)}) - E^2(y). \tag{16}$$

3. Results

3.1. Comparisons with in vivo measurements

Model validation is performed in twofold, with comparisons between simulated and measured results of: 1) waveforms in terms of normalized elastance, flow rate, and velocity for adults; and 2) age-related hemodynamic alterations in terms of stroke volume (SV), cardiac output (CO), mean systemic arterial pressure (MAP), heart rate (HR), mean pulmonary artery pressure, as well as left atrial and ventricular volumes, over a wide age range for infants, children, and adolescents.

Fig. 3 shows the comparison of the elastance, flow rate, and velocity waveforms between model simulations and experimental measurements [27–31]. The simulated hemodynamic waveforms for the adult model agree well with the *in vivo* measurements with similar waveform characteristics and amplitudes. Particularly, the important waveform features are well captured by the model in terms of, 1) a prominent antegrade flow during ventricular systole and a retrograde flow during early ventricular diastole as well as a small antegrade flow during ventricular diastole in ascending aorta and main pulmonary artery (Fig. 3c, d, e, f); and 2) a large antegrade flow during ventricular systole and a small antegrade flow during ventricular diastole as well as a small retrograde flow during right atrial contraction in vena cava (Fig. 3g, h, i, j). In Fig. 4 a comparison is made in terms of SV, CO, MAP, and HR for children aged 1–12 years [12], the simulations are capable of providing similar age-varying magnitudes and trends within a reasonable physiological range. Although the cardiac contractility, the afterload and the heart rate are observed to decrease with aging, CO increases with aging because of the increased SV. Fig. 5 shows a comparison of mean pulmonary arterial pressure (mP_{pua}) between simulations and measurements [32] for seven different age groups, the model predicted mP_{pua} shows seldom variations with aging, also is in good agreement with the measurements, pointing out an interesting phenomenon that mP_{pua} turns to maintain a relatively stable level during aging for healthy children. In Fig. 6 the simulated left atrial and ventricular volume waveforms during one cardiac circle are compared with the measurements among five different age groups [14], the simulated left atrial and ventricular time-volume curves during one cardiac cycle well match the measurements, indicating that left atrial and ventricular volumes increase with aging: the LV end-diastolic volume increases

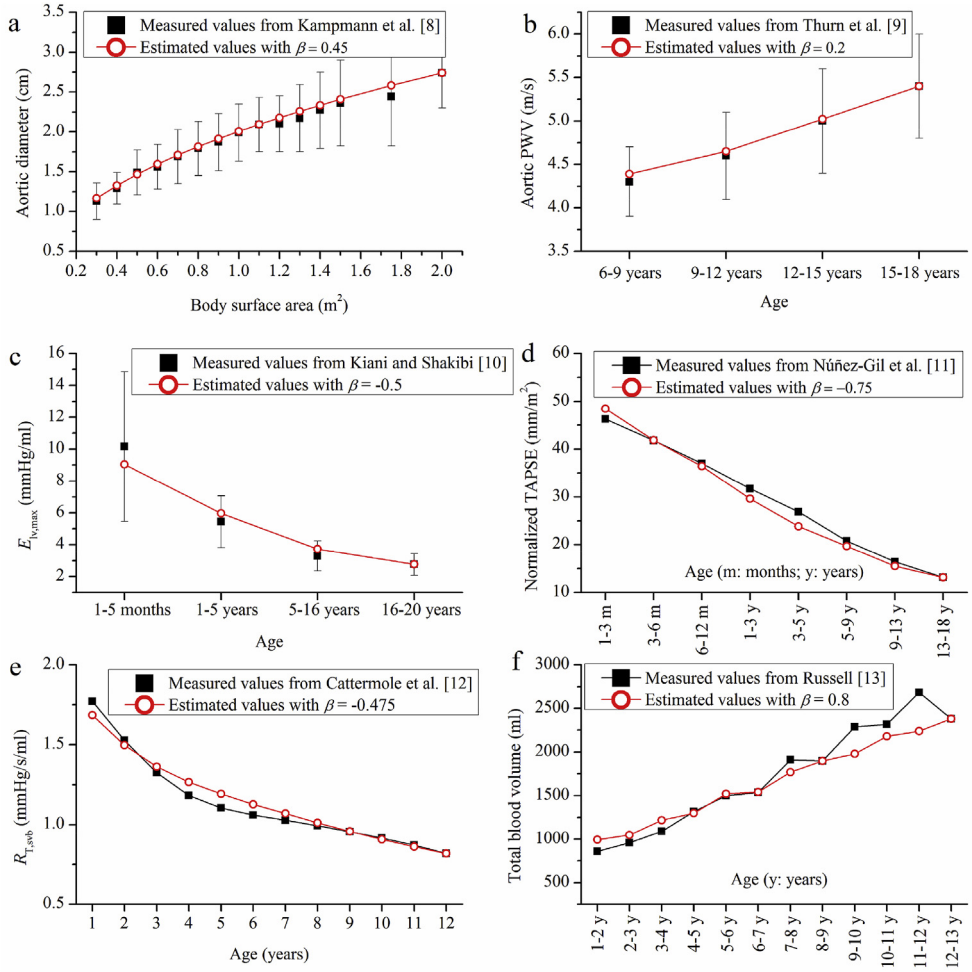

Fig. 2. Comparison of the cardiovascular parameter values between experimental measurements [8–13] and estimations with the defined β given in Table 1.

from 32.9 ml in the group aged 3.7 years up to as high as 112.1 ml in the group aged 17.3 years. It should be noted that a certain degree of discrepancy does exist in comparisons between experiment and simulation results, which is considered mainly due to the uncertainties of model simulations and experiments. Overall, age-related hemodynamics are predicted well agreeing with the measurements within reasonable physiological ranges, demonstrating the capability of the present generic multiscale cardiovascular model in predicting age-related hemodynamics for infants, children, and adolescents.

3.2. Global SA and uncertainty quantification (UQ)

For the healthy adult and the 3-year-old child with normal/abnormal circulation, we carried out an investigation on the main sensitivity indices of all cardiovascular parameters associated with the mostly interested model outputs: such as the mean ascending aortic pressure (mP_{as}), the mean inferior vena caval pressure (mP_{ivc}), the mean main pulmonary artery pressure (mP_{mpua}) or mean right pulmonary artery pressure (mP_{rpua}), and CO.

Fig. 7 compares the computed main sensitivity indices for the healthy adult model and the 3-year-old child model with the input uncertainties as given in Supplemental file 2. Similar values in the main sensitivity indices are observed between the two models. Generally, the main sensitivity index lower than 0.05 means the parameter has a negligible impact on the uncertainty of the model output. Thus, only parameters with main sensitivity indices higher than 0.05 are analyzed here. Fig. 8 compares the main sensitivity indices of selected important parameters. It is seen that the $R_{T,svb}$ has the most significant impact on the mP_{as} in all model inputs (Fig. 8a). The $D_{0,ivc}$, $c_{0,ivc}$, $P_{0,sv}$, and $E_{p,rv}$ play a primary role in affecting the mP_{ivc} (Fig. 8b). Influence of the p_{it} and $R_{T,svb}$ on the mP_{ivc} seems to be secondary (Fig. 8b). Compared with the adult model, the mP_{ivc} in the child model is more sensitive to $c_{0,ivc}$ and p_{it}, but less to $P_{0,sv}$, $R_{T,svb}$, and $E_{p,rv}$. With respect to mP_{mpua}, the $P_{0,sv}$, $R_{T,pvb}$, and $E_{p,rv}$ are obviously the primary impact parameters (Fig. 8c). The $D_{0,ivc}$, $c_{0,ivc}$, $E_{p,lv}$, and D_{tv} seems to be secondary (Fig. 8c). Compared with the adult model, the mP_{mpua} in the child model is more sensitive to $D_{0,ivc}$, $c_{0,ivc}$, $R_{T,pvb}$, and D_{tv}, but less to $P_{0,sv}$, $E_{p,rv}$, and $E_{p,lv}$. The CO is affected crucially by $D_{0,ivc}$, $P_{0,sv}$, p_{it}, $R_{T,svb}$, $E_{p,rv}$, $E_{p,lv}$, D_{tv}, t_{vcp}, and t_{ar} (Fig. 8d). Compared with the adult model, the CO in the child model is more sensitive to $D_{0,ivc}$, $P_{0,sv}$, p_{it}, D_{tv}, and t_{vcp}, but less to $R_{T,svb}$, $E_{p,rv}$, $E_{p,lv}$, and t_{ar}.

Fig. 9 compares the main sensitivity indices of selected important parameters between the health child model and the child model with the total cavopulmonary connection (TCPC) circulation. The TCPC circulation, as illustrated in Fig. 10, is normally built up through connecting the superior vena cava (SVC) to the right pulmonary artery (RPA) directly, and connecting the inferior vena cava (IVC) to the RPA via an artificial extracardiac conduit (EC). The TCPC circulation model developed here, only the cardiovascular structure is altered while keeping the model parameter values unchanged as those in the healthy 3-year-old child model. Such modification can facilitate the modeling of the intrinsic hemodynamic changes of the TCPC circulation caused by surgery-induced variations in the cardiovascular structure. The $R_{T,svb}$ and $P_{0,pua}$ are the primary and secondary important parameters on affecting the mP_{as} in the child model with the TCPC circulation. Compared with the healthy child model, the mP_{as} in the TCPC model is more

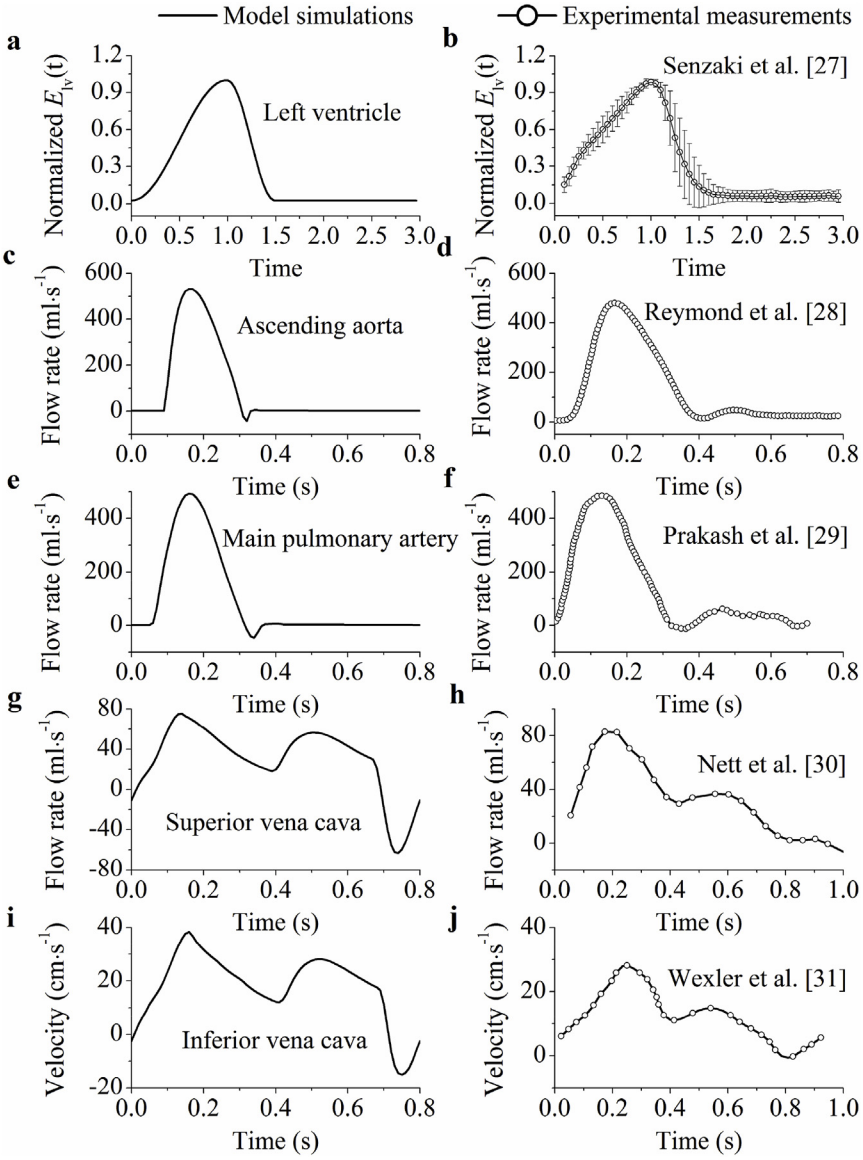

Fig. 3. Comparison between simulated and measured waveforms associated with adult circulation.

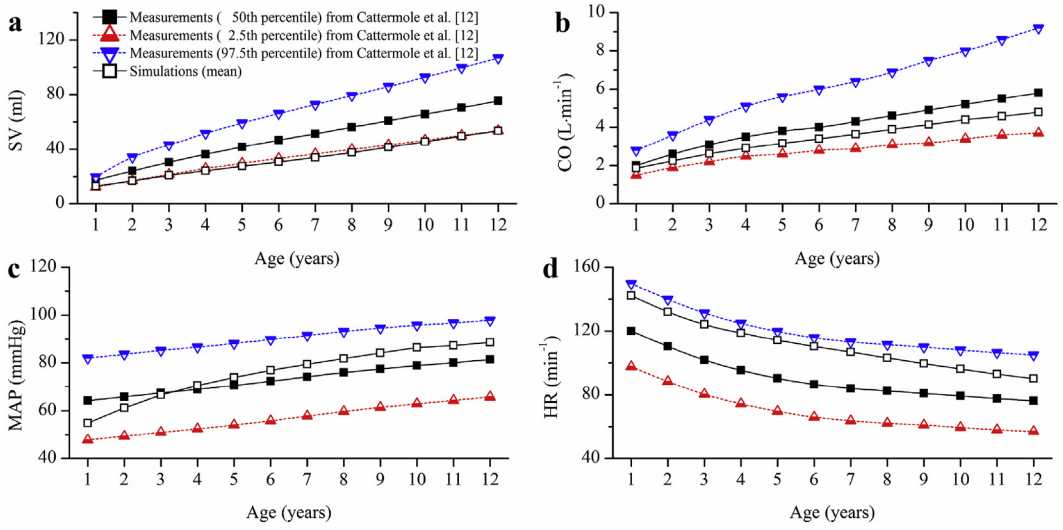

Fig. 4. Comparison between measured and simulated hemodynamics in children aged 1–12 years.

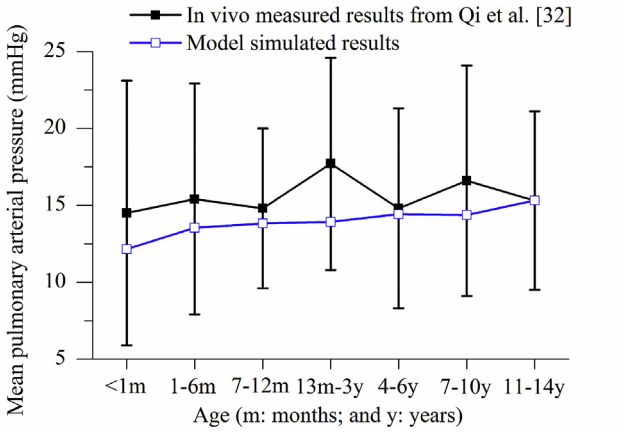

Fig. 5. Comparison between simulated and measured mean pulmonary arterial pressures in children aged from 1 month to 14 years.

sensitive to $P_{0,pua}$, but less to $P_{0,sv}$ and $R_{T,svb}$ (Fig. 9a). The $P_{0,sv}$ and $P_{0,pua}$ play a most important role on affecting mP_{ivc} and mP_{rpua} in the TCPC model, respectively (Fig. 9b and c). Compared with the healthy child model, the mP_{ivc} in the TCPC model is more sensitive to the $P_{0,sv}$ (Fig. 9b); the mP_{rpua} in the TCPC model is more sensitive to $P_{0,pua}$ (Fig. 9c). With respect to CO, the $P_{0,pua}$ is the primary impact parameter; p_{it}, $R_{T,pvb}$, and $E_{p,lv}$ are secondary impact parameters. Compared with the healthy child model, the CO in the TCPC model is more sensitive to $P_{0,pua}$, $R_{T,pvb}$, and $E_{p,lv}$, but less to $D_{0,ivc}$, $P_{0,sv}$, p_{it}, $R_{T,svb}$, and t_{vcp} (Fig. 9d).

Fig. 11 compares the computed probability density distributions of mP_{as}, mP_{ivc}, and CO for the TCPC model with the input uncertainties as in Supplemental file 2. Our results indicate that with a half reduction in the input uncertainties of $R_{T,svb}$, $P_{0,sv}$, and $P_{0,pua}$, i.e., the most influential model inputs, the uncertainties in the model outputs can be largely improved.

4. Discussion

In the following, we give an extensive discussion on several issues associated with the ASL-based computational modeling of the human CVS and global SA of the model parameters.

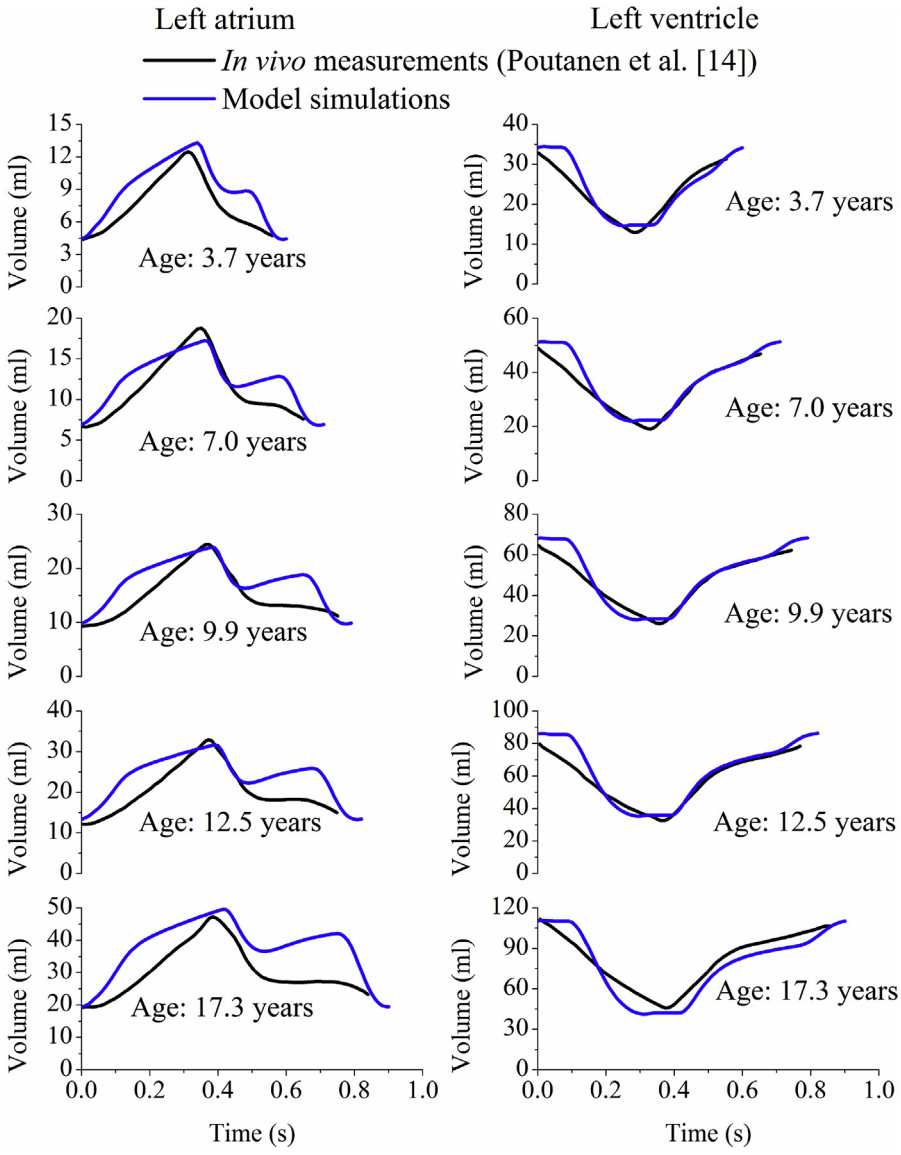

Fig. 6. Comparison between simulated and measured left atrial and ventricular volumes in children and young adults.

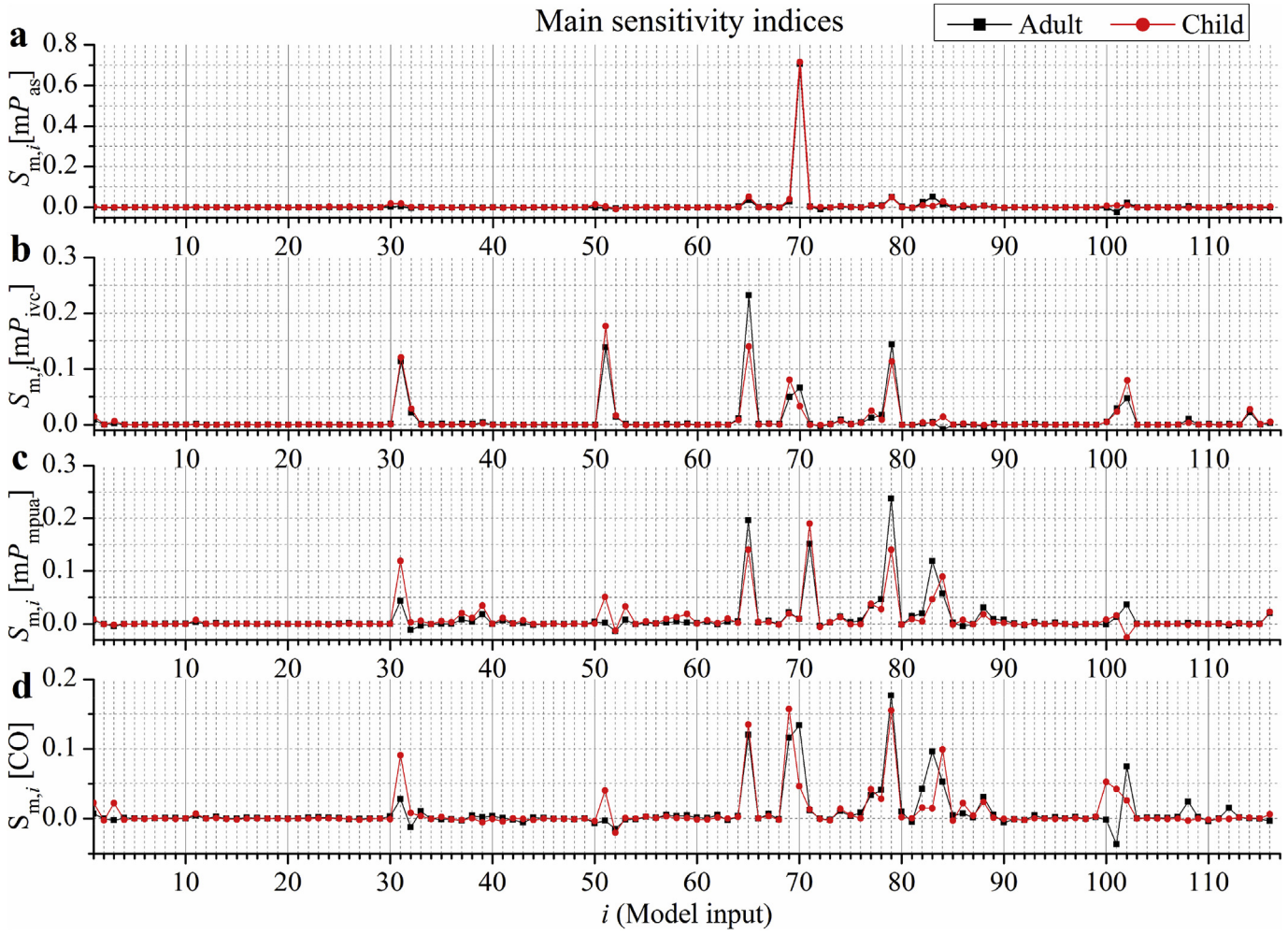

Fig. 7. Comparison of the computed main sensitivity indices between adult and 3-year-old child models. The corresponding number (*i*) to model inputs are given in Supplemental file 2.

4.1. ASL-based cardiovascular modeling

The scaling law of the mammalian CVS was first derived by West et al. [18], on the basis of that age-related changes in the size of the CVS obeys the ASL. Pennati and Fumero [19] made a definition of the scaling exponents to evaluate the fetal vascular and cardiac parameters, and investigated fetal hemodynamic changes associated with the gestational age. They found that the age-related cardiovascular parameters could be well predicted by applying the ASL-based scaling approach. In the ASL-based modeling, the scaling exponent (β) however turns to be a crucial parameter, which needs to be adjusted and determined reasonably corresponding to weight-dependent variations. After birth, age-related changes in both cardiovascular parameters and hemodynamics are significantly different from that of the fetus [8–17], particularly during the underage period [33,34], and thus it is necessary to redefine and adjust the scaling exponents (β) for different kinds of cardiovascular parameters. To the best of our knowledge, however, there have been no any studies on investigating the scaling exponents of evaluating age-related changes in the cardiovascular parameters across a wide age range, covering infants, children, and adolescents. In this study we for the first time successfully defined a sets of reasonable scaling exponents for different kinds of cardiovascular parameters covering infants, children, and adolescents. This was established based on the tremendous measurements from published literature, involving the cardiac elastance, the cardiac chamber volume, the heart rate, the diameters and lengths of the cardiac valves, the 1D vascular diameters and lengths, the pulse wave velocities, the compliance and resistance of the peripheral vascular bed, and the blood volume.

On the basis of clinical data, we applied $\beta = 0.45$ to evaluate the age-related changes in the cardiac valve and vascular dimensions, which shared a similar exponential association with the body size [35]. While Pennati and Fumero [19] suggested a value of $\beta = 0.33$ well describing the changes of the vascular diameters and lengths associated with the gestational age for the fetus, we found that $\beta = 0.45$ obviously led to a more accurate evaluation of the vascular diameters and lengths for infants, children, and adolescents. The predicted aortic diameters matched the echocardiographic measurements [8] excellently with a maximum percentage error of 5.7% (Fig. 2a). This indicates that the growth rate in cardiovascular dimensions should be different between prenatal and postnatal growth.

The aortic PWV, as an important predictor of the vascular stiffness, was observed to increase with aging in children and adolescents [9,36,37]. The measured aortic PWV increased from 4.3 m s^{-1} for 7-year-old males to 5.7 m s^{-1} for 19-year-old males [37]. We herein applied $\beta = 0.2$ to estimate the age-related changes in the PWV for systemic arteries, which was also observed to agree well with the *in vivo* measurements over a broad age range with a maximum percentage error of 1.1% [9] (Fig. 2b). Due to the paucity of data, in accordance with Mynard [38], we applied $\beta = 0.065$, $\beta = 0.075$, and $\beta = 0.065$ to evaluate the PWVs of the systemic veins, pulmonary arteries and veins, respectively. Note that the reference pressure P_0 was scaled with $\beta = 0.1$ for all 1D vessels.

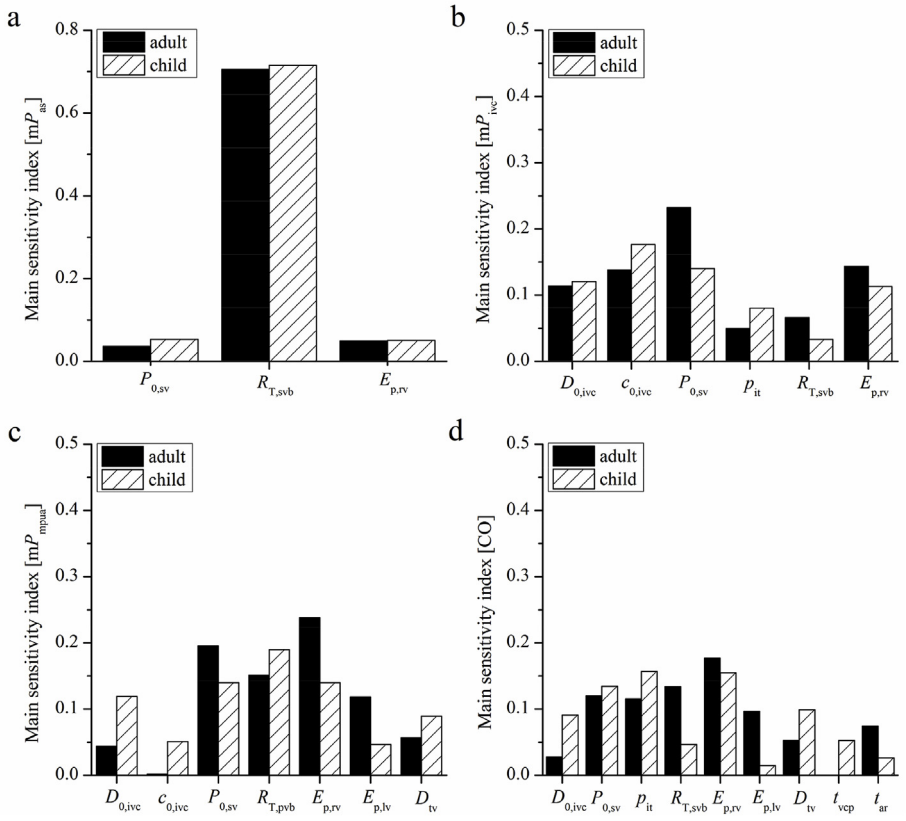

Fig. 8. Comparison of the main sensitivity indices higher than 0.05 between adult and 3-year-old child models.

Kiani and Shakibi [10] reported that the left ventricular end-systolic elastance ($E_{lv,max}$), which is a major determinant of representing the left ventricular systolic performance, decreased from 10.16 mmHg ml^{-1} in infants aged 1–12 months down to 2.76 mmHg ml^{-1} in young adults aged 16–20 years old. With $\beta = -0.5$ in our study, the predicted left ventricular elastance was in a reasonable agreement with *in vivo*

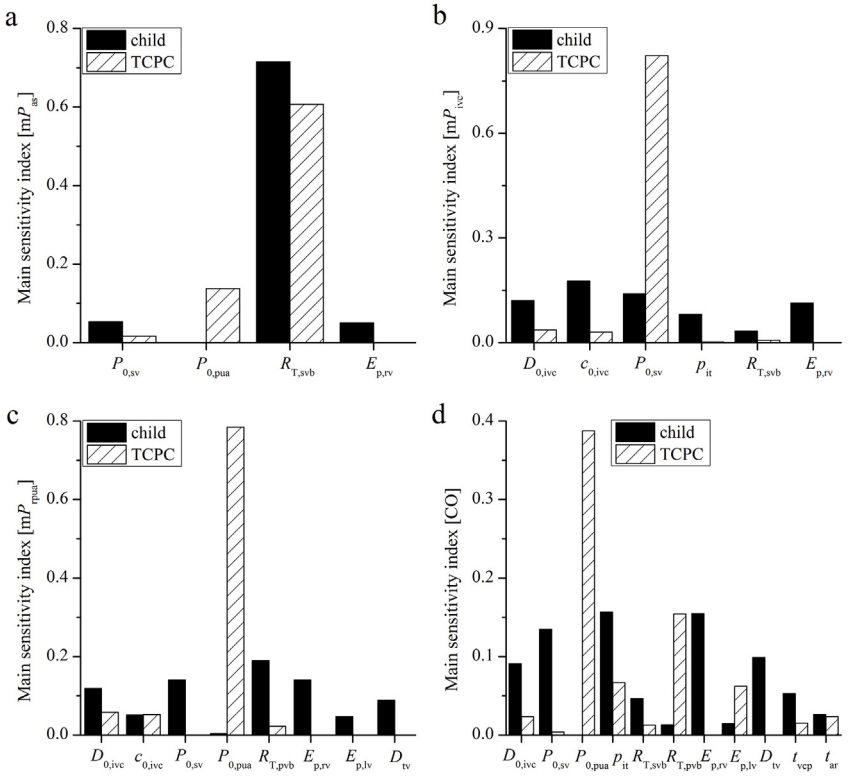

Fig. 9. Comparison of the main sensitivity indices higher than 0.05 between the 3-year-old child model and the child model with the TCPC circulation.

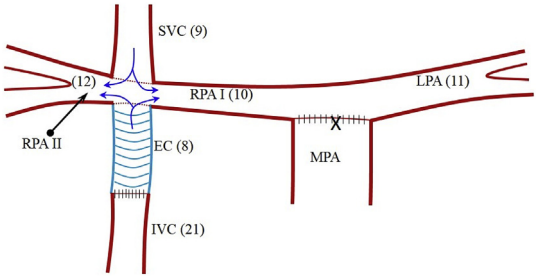

Fig. 10. Schematic representation of the TCPC connection.

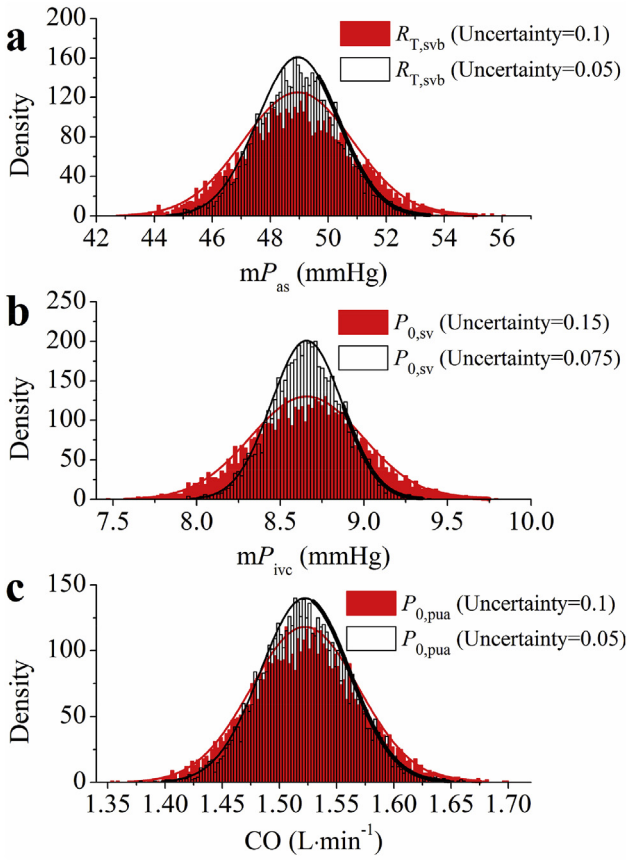

Fig. 11. Comparison of estimated probability density distributions for (a) mP_{as}, (b) mP_{ivc} and (c) CO. The probability density distributions are obtained by using the input uncertainties as presented in Supplemental file 2 (red) and half reduced values of input uncertainties in $R_{T,svb}$, $P_{0,sv}$, and $P_{0,pua}$, respectively (white).

measurements [10] (Fig. 2c). With respect to the right ventricular elastance, there is no study on evaluating the right ventricular elastance during aging to date. Measuring the tricuspid annular plane systolic excursion (TAPSE) has been a useful method to evaluate the right ventricular systolic functions. Núñez-Gil et al. [11] investigated the normalized TAPSE values associated with aging and found an aging-induced decrease in the right ventricular systolic performance. For the normalized TAPSE we herein found out that taking $\beta = -0.75$ over a broad range of 0–18 years (Fig. 2d) resulted in a good match with the measurements by a maximum percentage error of 11%. For left and right atrial elastances, because there are no measurements available yet, we may assume that they obey the similar scaling law in concern with the left and right ventricles, respectively.

With consideration of the fact that the total compliances of systemic and pulmonary circulations present a linear relationship with body weight [16], we herein adopted $\beta = 1.0$ to predict the compliances of peripheral vascular beds while utilizing $\beta = -0.475$ and $\beta = -0.7$ for the systemic and pulmonary vascular resistances, respectively. For a 6-month-old infant, $R_{T,pvb}$ was estimated to be 0.24 mmHg s·ml^{-1} within a reasonable range of 0.15–0.45 mmHg s·ml^{-1} [39]. Furthermore, the systemic vascular resistance ($R_{T,svb}$) was estimated with $\beta = -0.475$, matching well the *in vivo* measurements [12] with a maximum percentage error of 8% (Fig. 2e); the total blood volume with $\beta = 0.8$ showed a reasonable agreement with the measurements [13] with a maximum percentage error of 16.5% (Fig. 2f).

In Table 1 a set of scaling exponents were summarized, which were validated to be capable of estimating different cardiovascular parameters (Fig. 2), indicating that the present ASL-based approach could be a versatile and useful method for the prediction of age-related cardiovascular parameters. With application of the scaling law based on the defined scaling exponents (Table 1), we then investigated the hemodynamic changes associated with age for infants, children, and adolescents, in which reasonable agreement was observed between the simulations and measurements in all cases [Figs. 4–6]. This demonstrates the feasibility and validity of the currently proposed cardiovascular model in predicting the age-related alterations in cardiovascular parameters and hemodynamics over a broad parameter space, involving the cardiac contractility, the cardiac chamber volume, the heart rate, the diameters and lengths of the cardiac valves, the 1D vascular diameters and lengths, the pulse wave velocities, the compliance and resistance of the peripheral vascular bed, and the blood volume.

4.2. Global SA

The uncertainties of model inputs caused by empirical estimations or experimental measurements may result in the uncertainties of model outputs. We carried out a variance-based global SA to evaluate the most influential parameters in the adult and the children models with normal/abnormal circulations. Due to the lack of sufficient data to define probability density functions for the model inputs, all model parameters are assumed to be normal distributions in their uncertain domains, as summarized in Supplemental file 2. It is reasonable because almost all of the adult model parameters are taken from published literature and have the highest probability to approach their expected values [40]. All cardiovascular parameters are further assumed to be mutually independent.

With consideration of the complexity of the 0-1D multiscale cardiovascular model and its large number of model inputs, we herein utilized the Monte Carlo-based method for SA. The merit is that the existing computational code can be employed straightforward without any modifications [41]. Furthermore, since the random sample-based evaluation of the sensitivity indices is computationally expensive, the LHS technique was utilized to generate stratified random samples for model inputs [25]. The Saltelli's efficient procedure [26] was further used to evaluate the main sensitivity indices, which significantly reduced the total number of model evaluations from $2kn^2$ to $n(k+2)$.

Our results showed that there are no distinctive discrepancies in the main sensitivity indices between the healthy adult and 3-year-old child models (Fig. 7), considerably because of the utilization of the same cardiovascular structure designs. For the 3-year-old child model with the TCPC circulation, as a result of the significant alterations in cardiovascular structure, the main sensitivity indices however distinguish remarkably from those of the healthy child model (Fig. 9). Interestingly, our study reveals that eleven primary cardiovascular parameters show the highest sensitivity in the multiscale cardiovascular modeling, involving the total systemic peripheral vascular resistance, the total pulmonary peripheral vascular resistance, the reference pressure, the diameter, the pulse wave velocity of the 1D vena cava, the left and right ventricular passive elastance, the duration of ventricular contraction, the time of the atrial relaxation, the intrathoracic pressure, the diameter of tricuspid valve. It should be noted that the eleven model parameters

are highest sensitivity indices for the model outputs of mP_{as}, mP_{ivc}, mP_{mpua}, and CO, respectively. It may be possible that other input parameters might be more sensitive when one investigates other model outputs of interests. It is therefore reasonable to think that, in order to provide more accurate and reliable model predictions for clinical decision-making, an extensive parameter-based study should be focused specifically on the issue, which may improve the accuracy and performance of the multiscale modeling of the CVS.

4.3. Limitations and future work

For simplification, only twenty larger vessels are represented by 1D models while the reminder vessels are lumped into the peripheral vascular beds. Thus, the present model cannot provide detailed hemodynamic predictions for other vascular compartments, such as cerebral and hepatic circulations. In principle, the model however can be easily expanded to a fine multiscale cardiovascular model covering most of the large arteries (55 vessels) and veins (72 vessels) as in our previous study [5], which is one of our future works.

The cardiovascular parameter values for infants, children, and adolescents are converted from the adult model by introducing the ASL-based approach in a manner of the population-averaged data. For clinical applications of personalized medicine, the model parameters should be personalized based on various inputs of patient-specific data. However, it is infeasible to define all of model parameters with direct measurements in the simulation. We need to achieve an optimal trade-off between experimental measurements and population-averaged data-based parameter estimations. Therefore, SA and UQ is necessary to identify the most important model parameters and quantify the possible errors resulted from uncertainties of model parameters. In the SA, the probability density functions for all of the cardiovascular parameters are assumed to be normal distributions. Taking into account the realistic probability density functions based on measurements and quantifying their influence on the global SA needs to be further studied in detail.

5. Conclusions

In this study we introduced the ASL-based approach and proposed a set of the scaling exponents to specifically describe different types of cardiovascular parameters for juveniles, and successfully established a novel closed-loop 0-1D multiscale cardiovascular model applicable to a wide range of age groups. The model was validated to be capable of predicting age-related alterations in both cardiovascular parameters and hemodynamics for healthy infants, children, and adolescents with consideration of the cardiovascular growth and development during aging. Uncertainties in modeling hemodynamics of the healthy adult and the 3-year-old children with/without TCPC circulation were further quantified through a global SA, indicating that surgically-created structures associated with TCPC circulation will cause distinct discrepancies in sensitivity indices whereas growth-induced alterations in cardiovascular parameters have a negligible impact. Our results demonstrated that the present cardiovascular model is versatile and robust, providing a generic and age-specific method for simulation-based predictive medicine in terms of pathophysiologic mechanisms exploration and clinical interventions.

Conflicts of interest

None Declared.

Acknowledgements

XZ acknowledges the support from the Institute for Global Prominent Research, Chiba University, Japan. HL was partly supported by Grant-in-Aid for Scientific Research (17300141), JSPS.

Appendix. Adult model parameters of the closed-loop 0-1D multiscale cardiovascular model

Table A.1
Geometrical and mechanical characteristics of the 1D cardiovascular network in modeling of the adult circulation [2].

NO.	Vessel	*Len* (cm)	D_0 (cm)	c_0 (m·s^{-1})	P_0 (mmHg)
1	AscAo	4.0	2.94	4.60	80
2	AoArc I	2.0	2.58	4.60	80
3	BCA	3.4	1.40	4.64	80
4	AoArc II	3.9	2.48	4.60	80
5	LCA	3.4	0.74	5.29	80
6	LSA	3.4	1.09	4.75	80
7	DTA	5.2	2.20	4.60	80
8	IVC	7.0	2.20	1.38	5
9	SVC	6.0	1.80	1.48	5
10	MPA	4.3	2.70	2.77	11
11	LPA	2.5	1.80	2.80	11
12	RPA	5.8	2.20	2.78	11
13	LSPA	1.2	0.96	3.24	11
14	LIPA	2.1	1.69	2.81	11
15	RSPA	1.9	1.51	2.84	11
16	RIPA	2.4	1.85	2.79	11
17	LSPV	1.2	1.43	1.35	6
18	LIPV	2.1	1.28	1.43	6
19	RSPV	1.9	1.65	1.27	6
20	RIPV	2.4	1.73	1.25	6

Table A.2

Parameters of peripheral vascular beds in modeling of the adult circulation.

Systemic vascular bed
$R_{T,svb}$ = 0.9 mmHg s·ml^{-1}, $C_{T,sa}$ = 1.7 ml mmHg^{-1}, $C_{T,sv}$ = 146.0 ml mmHg^{-1} [2].

Artery	C_{sa} (ml·mmHg^{-1})	R_{svb} (mmHg·s·ml^{-1})	C_{sv} (ml·mmHg^{-1})	Vein
3	0.243	4.66	44.22	9
5	0.066	17.31		
6	0.079	14.06		
7	0.891	1.30	98.89	8

Pulmonary vascular bed
$R_{T,pvb}$ = 0.05 mmHg s·ml^{-1}, $C_{T,pua}$ = 5.7 ml mmHg^{-1}, $C_{T,puv}$ = 15.8 ml mmHg^{-1} [2].

Artery	C_{pua} (ml·mmHg^{-1})	R_{pvb} (mmHg·s·ml^{-1})	C_{puv} (ml·mmHg^{-1})	Vein
13	0.673	0.56	1.476	17
14	1.901	0.19	5.832	18
15	1.862	0.20	4.528	19
16	2.934	0.13	7.598	20

Table A.3
Parameters of cardiac chambers and valves in modeling of the adult circulation [2,5,24].

Cardiac chambers	ra	rv	la	lv
E_a (mmHg·ml^{-1})	0.3	1.2	0.35	3.0
E_p (mmHg·ml^{-1})	0.1	0.08	0.2	0.08
V_0 (ml)	5.0	10.0	5.0	10.0
V_{ini} (ml)	25.0	120.0	25.0	120.0
S (mmHg·s·ml^{-1})	$\phi_S p_{ra}$	$\phi_S p_{rv}$	$\phi_S p_{la}$	$\phi_S p_{lv}$
Cardiac valves	tv	pv	mv	av
$A_{eff,max}$ (cm^2)	6.0	5.7	5.1	4.9
$A_{eff,min}$ (cm^2)	0.0	0.0	0.0	0.0
l_{eff} (cm)	2.0	1.5	2.0	1.5
K_{vo} (mmHg^{-1}·s^{-1})	16.0	13.3	16.0	17.3
K_{vc} (mmHg^{-1}·s^{-1})	16.0	20.0	16.0	17.3

Appendix A. Supplementary data

Supplementary data to this article can be found online at https://doi.org/10.1016/j.compbiomed.2019.03.021.

References

[1] F. Liang, et al., Multi-scale modeling of the human cardiovascular system with applications to aortic valvular and arterial stenosis, Med. Biol. Eng. Comput. 47 (7) (2009) 743–755.
[2] J.P. Mynard, J.J. Smolich, One-dimensional haemodynamic modeling and wave dynamics in the entire adult circulation, Ann. Biomed. Eng. 43 (6) (2015) 1443–1460.
[3] L.O. Müller, E.F. Toro, Enhanced global mathematical model for studying cerebral venous blood flow, J. Biomech. 47 (13) (2014) 3361–3372.
[4] M.U. Qureshi, et al., Numerical simulation of blood flow and pressure drop in the pulmonary arterial and venous circulation, Biomechanics Model. Mechanobiol. 13 (5) (2014) 1137–1154.
[5] X. Zhang, et al., Gravitational effects on global hemodynamics in different postures: a closed-loop multiscale mathematical analysis, Acta Mech. Sin. 33 (3) (2017) 595–618.
[6] A. Kempny, et al., Outcome of cardiac surgery in patients with congenital heart disease in England between 1997 and 2015, PLoS One 12 (6) (2017) e0178963.
[7] S. Nayak, P.D. Booker, The fontan circulation, Cont. Educ. Anaesth. Crit. Care Pain 8 (1) (2008) 26–30.
[8] C. Kampmann, et al., Normal values of M mode echocardiographic measurements of more than 2000 healthy infants and children in central Europe, Heart 83 (6) (2000) 667–672.
[9] D. Thurn, et al., Aortic pulse wave velocity in healthy children and adolescents: reference values for the vicorder device and modifying factors, Am. J. Hypertens. 28 (12) (2015) 1480–1488.
[10] A. Kiani, J.G. Shakibi, Normal value of left ventricular end-systolic elastance in infants and children, Iran, J. Med. Sci. 28 (4) (2015) 169–172.
[11] I.J. Núñez-Gil, et al., Determination of normalized values of the tricuspid annular plane systolic excursion (TAPSE) in 405 Spanish children and adolescents, Rev. Esp. Cardiol. 64 (8) (2011) 674–680.
[12] G.N. Cattermole, et al., The normal ranges of cardiovascular parameters in children measured using the Ultrasonic Cardiac Output Monitor, Crit. Care Med. 38 (9) (2010) 1875–1881.
[13] S.J. Russell, Blood volume studies in healthy children, Arch. Dis. Child. 24 (118) (1949) 88–98.
[14] T. Poutanen, et al., Left atrial and left ventricular function in healthy children and young adults assessed by three dimensional echocardiography, Heart 89 (5) (2003) 544–549.
[15] M.S.J. Sutton, et al., Effect of age related changes in chamber size, wall thickness, and heart rate on left ventricular function in normal children, Heart 48 (4) (1982) 342–351.
[16] F. Liang, et al., Hemodynamic performance of the Fontan circulation compared with a normal biventricular circulation: a computational model study, Am. J. Physiol. Heart Circ. Physiol. 307 (7) (2014) H1056–H1072.
[17] H. Senzaki, et al., Age-associated changes in arterial elastic properties in children, Eur. J. Pediatr. 161 (10) (2002) 547–551.
[18] G.B. West, J.H. Brown, B.J. Enquist, A general model for the origin of allometric scaling laws in biology, Science 276 (5309) (1997) 122–126.
[19] G. Pennati, R. Fumero, Scaling approach to study the changes through the gestation of human fetal cardiac and circulatory behaviors, Ann. Biomed. Eng. 28 (4) (2000) 442–452.
[20] J. Alastruey, et al., On the impact of modelling assumptions in multi-scale, subject-specific models of aortic haemodynamics, J. R. Soc. Interface 13 (119) (2016) 20160073.
[21] W.L. Maughan, K. Sunagawa, K. Sagawa, Ventricular systolic interdependence: volume elastance model in isolated canine hearts, Am. J. Physiol. Heart Circ. Physiol. 253 (6) (1987) H1381–H1390.
[22] Y. Sun, et al., A comprehensive model for right-left heart interaction under the influence of pericardium and baroreflex, Am. J. Physiol. Heart Circ. Physiol. 272 (3) (1997) H1499–H1515.
[23] J.P. Mynard, et al., A simple, versatile valve model for use in lumped parameter and one-dimensional cardiovascular models, Int. J. Numer. Meth. Biomed. 28 (6–7) (2012) 626–641.
[24] X. Zhang, et al., Cardiovascular disease-induced thermal responses during passive heat stress: an integrated computational study, Int. J. Numer. Meth. Biomed. 32 (11) (2016) e02768.

[25] G.D. Wyss, K.H. Jorgensen, A Users Guide to LHS: Sandias Latin Hypercube Sampling Software, Sandia National Labs., Albuquerque, NM (United States), 1998 (No. SAND-98-0210).
[26] A. Saltelli, Making best use of model evaluations to compute sensitivity indices, Comput. Phys. Commun. 145 (2) (2002) 280–297.
[27] H. Senzaki, C.H. Chen, D.A. Kass, Single-beat estimation of end-systolic pressure-volume relation in humans: a new method with the potential for noninvasive application, Circulation 94 (10) (1996) 2497–2506.
[28] P. Reymond, et al., Validation of a one-dimensional model of the systemic arterial tree, Am. J. Physiol. Heart Circ. Physiol. 297 (1) (2009) H208–H222.
[29] A. Prakash, et al., Faster flow quantification using sensitivity encoding for velocity-encoded cine magnetic resonance imaging: in vitro and in vivo validation, J. Magn. Reson. Imaging 24 (3) (2006) 676–682.
[30] E.J. Nett, et al., Four-dimensional phase contrast MRI with accelerated dual velocity encoding, J. Magn. Reson. Imaging 35 (6) (2012) 1462–1471.
[31] L. Wexler, et al., Velocity of blood flow in normal human venae cavae, Circ. Res. 23 (3) (1968) 349–359.
[32] H.Y. Qi, et al., Anatomical and hemodynamic evaluations of the heart and pulmonary arterial pressure in healthy children residing at high altitude in China, IJC Heart Vasc. 7 (2015) 158–164.
[33] G. de Simone, et al., Interaction between body size and cardiac workload: influence on left ventricular mass during body growth and adulthood, Hypertension 31 (5) (1998) 1077–1082.
[34] C. Wu, et al., Age-related changes of normal cerebral and cardiac blood flow in children and adults aged 7 months to 61 years, J. Am. Heart Assoc. 5 (1) (2016) e002657.
[35] T. Sluysmans, S.D. Colan, Theoretical and empirical derivation of cardiovascular allometric relationships in children, J. Appl. Physiol. 99 (2) (2005) 445–457.
[36] E.V. Hidvégi, et al., Reference values of aortic pulse wave velocity in a large healthy population aged between 3 and 18 years, J. Hypertens. 30 (12) (2012) 2314–2321.
[37] G.S. Reusz, et al., Reference values of pulse wave velocity in healthy children and teenagers, Hypertension 56 (2) (2010) 217–224.
[38] J.P. Mynard, Computer Modelling and Wave Intensity Analysis of Perinatal Cardiovascular Function and Dysfunction (Doctoral dissertation), (2011).
[39] J.A. Goodwin, et al., A model for educational simulation of infant cardiovascular physiology, Anesth. Analg. 99 (6) (2004) 1655–1664.
[40] P. Chen, A. Quarteroni, G. Rozza, Simulation-based uncertainty quantification of human arterial network hemodynamics, Int. J. Numer. Meth. Biomed. 29 (6) (2013) 698–721.
[41] V.G. Eck, et al., A guide to uncertainty quantification and sensitivity analysis for cardiovascular applications, Int. J. Numer. Meth. Biomed. 32 (8) (2016) e02755.

Hao Liu is professor of mechanical engineering at Chiba University. He was a senior research scientist in RIKEN (2000–2003), an assistant professor in Nagoya Institute of Technology (1998–2000), a research scientist in Japan Science and Technology Agency (JST) (1993–1997), and a research scientist in Ship Research Institute (1992–1993). He received a BS degree from Dalian University of Technology in 1985 and received his MS and PhD degrees, both in fluid engineering, in 1989 and in 1992, respectively. He is the author and a co-author of more than 190 papers in refereed journals with more than 6200 citations (Google Scholar), mainly dealing with computational mechanics, biomechanics in flying and swimming, fluid-structure interaction, biomimetics, insect-inspired micro air vehicles, and bio-inspired engineering as well as multi-scale, multi-physical modeling of the cardiovascular system, and predictive medicine. He is an associate editor-in-chief of *Acta Mechanica Sinica* and associate editors of *Biomimetics & Bioinspiration* and *Journal of Bionics Engineering*.